13 DMFT and GW+DMFT for Systems out of Equilibrium

Martin Eckstein
University of Erlangen-Nürnberg
91058 Erlangen, Germany

Contents

E. Pavarini, E. Koch, A. Lichtenstein, and D. Vollhardt (eds.)
Dynamical Mean-Field Theory of Correlated Electrons
Modeling and Simulation Vol. 12
Forschungszentrum Jülich, 2022, ISBN 978-3-95806-619-9
http://www.cond-mat.de/events/correl22

1 Introduction

Pump-probe experiments with short laser pulses allow to excite condensed matter systems and to spectroscopically analyze the subsequent dynamics of their microscopic degrees of freedom over a wide range of timescales, from fast electronic processes below one femtosecond to the picosecond dynamics of the crystal lattice and of collective orders like superconductivity. Femtosecond pulses are nowadays available in a large spectrum of photon energies, and many complementary probing techniques have been brought to the ultrafast time domain: For example, time- and angular-resolved photoemission (trARPES) can probe the momentum-dependent electronic structure, time-resolved Xray scattering can reveal the evolution of the crystal lattice, and resonant inelastic Xray scattering (RIXS) based on intense Xray pulses from free electron laser sources can give access to low energy magnetic and orbital excitations. Such experiments have opened up a field of research in condensed matter physics with many facets [1–3]: On the one hand, the hope is that a real-time observation of dynamical processes can reveal the interaction between microscopic degrees of freedom more directly than conventional equilibrium probes. On the other hand, many experiments have shown that an excitation of correlated solids far out of equilibrium can give rise to states that are not simply related to equilibrium phase diagram, which suggests the possibility for a controlled engineering of the collective behavior in solids on ultrafast timescales.

In general, we can distinguish two classes of pathways used to establish new equilibrium states. First, the redistributions of electron populations between different bands and orbitals can trigger a nontrivial dynamics. This redistribution is often loosely referred to as photo-doping, although it does not imply a change of the total electron count (like in chemical doping), but only a change of the electron count in a certain subset of bands. Such photo-excitation processes have been shown to, e.g., induce a metal-insulator transition in VO_2 on timescales below 100 fs [4], lead to the enhancement of excitonic condensates [5], or trigger photo-induced non-thermal phase transitions like the photo-induced melting of antiferromagnetic order [6]. In strongly correlated electron systems, photo-doping can have a direct impact on the electronic structure, due to a shift of the bands, the formation or destruction of coherent quasiparticles, and the ultrafast modification of relevant interaction parameters due to screening, such as the Hubbard U (see Sec. 4.1). The second pathway relies on a direct effect of the laser field while a system is driven. This includes the idea of nonlinear phononics [7], where the anharmonic coupling to strongly driven phonon modes is used to steer the crystal lattice, but also the magnetic and electronic properties of solids. More generally, the period-averaged dynamics of a periodically driven system can be understood in terms of a so-called Floquet Hamiltonian, which can differ significantly from the un-driven Hamiltonian in the presence of nonlinearities. A prominent example of this so-called Floquet engineering, which is more routinely used in cold atom experiments [10], is the generation of topologically nontrivial bands by circularly polarized light in graphene [8, 9], and there are many theoretical proposals towards Floquet engineering of interacting quantum systems, such as a manipulation of superconducting pairing or spin-exchange interactions [2, 3]. In a solid, however, heating processes from the drive are usually inevitable,

so that properties of the driven state rely both on the field-induced modification of the Hamiltonian, and on the effect of non-thermal electron populations similar to photo-doping.
The theoretical description of such non-equilibrium processes must therefore capture the joint evolution of the spectrum (density of states) and the distribution functions, which mutually depend on each other in a correlated system. The Keldysh formalism provides the framework to discuss many-body physics for transient and steady-state non-equilibrium situations. Technically, many-body approaches which are rooted in a diagrammatic formalism can be generalized to the time-domain by replacing imaginary-time arguments by a time variable on a more general real-time contour. In particular, this holds for dynamical mean-field theory (DMFT) [11–14] and its extensions, which in equilibrium present a versatile approach to obtain the electronic structure of correlated electrons. The numerical evaluation of the resulting equations in real-time is however far more challenging, as discussed below. In the context of DMFT, the main challenge is the non-perturbative solution of the quantum impurity problem: Real-time Quantum Monte Carlo techniques have to cope with the notorious dynamical sign problem, while wave-function based techniques such as matrix product state evolutions suffer from the full exponentially large dimension of the relevant Hilbert space (see Sec. 3.2). In spite of that, non-equilibrium DMFT is applied to an increasing set of topics in particular related to the study of photo-induced dynamics in Mott insulators, e.g., to understand light-induced phases such as hidden states with spin and orbital order [15] or superconductivity [16], or the investigation of strong-field phenomena such as strong-field localization and high-harmonic generation [17,18].
The purpose of this lecture is to explain the foundations of non-equilibrium DMFT and some of its extensions, more than giving a summary of recent applications. As such, the lecture has a significant overlap with a previous lecture in this school [19]. Nevertheless, in order to provide a self-contained set of notes we will repeat some of the basic concepts. Compared to the previous lecture, the present notes do not contain details of the solution of integral equations for real-time non-equilibrium Green functions (there is now a detailed technical report on this in the literature [20]), but instead include a chapter on the GW+DMFT formalism out of equilibrium, which is a promising route towards first principles simulations of correlated electron systems out of equilibrium.

2 Keldysh formalism

This chapter recapitulates basis aspects of the Keldysh formalism. For a more detailed review, the reader might consider the textbooks by Kamenev [21], Stefanucci and van Leeuwen [22], or Ref. [14].

2.1 The L-shaped time contour

Time evolution operator

We consider a system which at initial time t_0 is in a given quantum state, or more generally a statistical mixture $\rho = \sum_n w_n |\psi_n\rangle\langle\psi_n|$ of states $|\psi_n\rangle$ with probabilities w_n. In the follow-

ing, we will assume the latter to be the thermal Gibbs ensemble for a given Hamiltonian, $\rho = e^{-\beta H(t_0)}/Z$. For times $t > t_0$, the system then evolves according to a time-dependent Hamiltonian $H(t)$. Taking the expectation value of an observable O in the time-evolved state and averaging over initial states gives

$$\langle O(t)\rangle = \sum_n w_n \langle\psi_n|\,\mathcal{U}(t_0,t)\,O\,\mathcal{U}(t,t_0)|\psi_n\rangle = \mathrm{Tr}\,\rho\mathcal{U}(t_0,t)\,O\,\mathcal{U}(t,t_0)\,, \tag{1}$$

with the time-evolution operator $\mathcal{U}(t,t')$ from time t' to t. For $t > t'$ (forward evolution), the latter is given by ($\hbar = 1$ throughout these notes)

$$\mathcal{U}(t,t') = T_t\, e^{-i\int_{t'}^t d\bar{t}\, H(\bar{t})}, \tag{2}$$

where T_t is the time-ordering operator which brings operators at later time to the left. The action of the time-ordering can be read in two ways: First, by splitting the time-interval $[t',t]$ in $N\to\infty$ infinitesimal time-steps ($t_0 \equiv t', t_1, ..., t_N = t$), over which the Hamiltonian can be taken to be constant, we have

$$T_t\, e^{-i\int_{t'}^t d\bar{t} H(\bar{t})} = T_t \lim_{N\to\infty}\prod_{j=1}^{N} e^{-i(t_j-t_{j-1})H(t_j)} = \lim_{N\to\infty} e^{-i(t_N-t_{N-1})H(t_N)}\cdots e^{-i(t_1-t_0)H(t_1)}, \tag{3}$$

i.e., the time-ordering operator brings the evolution over the infinitesimal time-steps $[t_j, t_{j+1}]$ in the correct order. Alternatively, we can expand the exponent in Eq. (2) in a Taylor series and apply the time-ordering to the individual terms,

$$T_t\, e^{-i\int_{t'}^t d\bar{t} H(\bar{t})} = \sum_{n=0}^{\infty}\frac{(-i)^n}{n!}\int_{t'}^t dt_1\cdots\int_{t'}^t dt_n\, T_t\Big(H(t_1)\cdots H(t_n)\Big) \tag{4}$$

$$= 1 + \sum_{n=1}^{\infty}(-i)^n\int_{t'}^t dt_1\int_{t'}^{t_1} dt_2\cdots\int_{t'}^{t_{n-1}} dt_n\, H(t_1)\cdots H(t_n). \tag{5}$$

This expression is recognized as iterative solution of the integral equation for the evolution operator, $\mathcal{U}(t,t') = 1 + \int_{t'}^t dt_1 H(t_1)\mathcal{U}(t_1,t')$.

L-shaped time-contour and contour-ordered correlation functions

With an analogous notation, the backward time-evolution can be expressed using the anti time-ordering operator $T_{\bar{t}}$ that brings operators at later time to the right, $\mathcal{U}(t',t) = T_{\bar{t}}\, e^{-i\int_{t'}^t d\bar{t} H(\bar{t})}$ for $t' < t$. Finally, writing the density matrix ρ in terms of the imaginary time evolution with $H(\tau) \equiv H(0)$, the expectation value Eq. (1) becomes

$$\mathrm{Tr}\,\rho\mathcal{U}(t_0,t)\,O\,\mathcal{U}(t,t_0) \;= \frac{1}{Z}\,\mathrm{Tr}\left(T_\tau e^{-\int_0^\beta d\tau H(\tau)}\right)\left(T_{\bar{t}} e^{-i\int_t^0 dt H(t)}\right)O\left(T_t e^{-i\int_0^t dt H(t)}\right). \tag{6}$$

(Here and in the following we set $t_0 = 0$ without loss of generality). The three time-ordered exponentials in this expression can be combined into a single time-ordering along the L-shaped

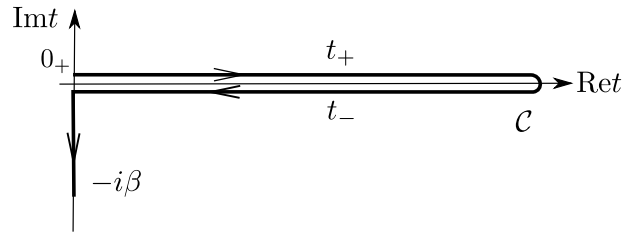

Fig. 1: *The Keldysh contour $\mathcal{C}$, ranging from time 0 to a maximum time t_{max}, back to time 0, and finally to $-i\beta$ on the imaginary-time branch. Times on the upper and lower real-time branch are denoted by t_+ and t_-, respectively. Both t_+ and t_- are real, and the index $\pm$ serves only to distinguish backward and forward time-evolution. The arrows denote the time-ordering along $\mathcal{C}$ from "earlier" to "later" contour times.*

time contour $\mathcal{C}$, which extends from 0 to some maximum time $t_{\max}$ in forward direction, back to 0, and finally to $-i\beta$ in the imaginary direction (see Fig. 1). Hence, Eq. (6) becomes

$$\langle \mathcal{O}(t) \rangle = \frac{1}{Z} \operatorname{Tr} T_{\mathcal{C}}\, e^{-i\int_{\mathcal{C}} dt H(t)} O(t), \tag{7}$$

with the contour-ordering operator

$$T_{\mathcal{C}} A(t)B(t') = \begin{cases} A(t)B(t') & t \text{ later than } t' \text{ on } \mathcal{C} \\ \xi B(t')A(t) & t' \text{ later than } t \text{ on } \mathcal{C}. \end{cases} \tag{8}$$

The sign ξ is -1 if the permutation of A and B involves an odd number of permutations of fermion creation of annihilation operators, and $+1$ otherwise. The sign is not relevant in Eq. (7), but only for the definition of correlation functions below. Equations (7) and (3) are then understood in the same way: splitting the contour in $N \to \infty$ infinitesimal steps ($t_0 \equiv 0_+, t_1, ..., t_N = -i\beta$), with $t_o = t_+$ being the time argument of the operator O, the operator $T_{\mathcal{C}}$ in the expression

$$T_{\mathcal{C}}\Big(e^{-i\int_{\mathcal{C}} dt H(t)} O(t)\Big) = T_{\mathcal{C}}\Big(\prod_{j=1}^{N} e^{-i(t_j - t_{j-1})H(t_j)} O(t_o)\Big) \tag{9}$$

orders the evolution over the infinitesimal timesteps $[t_j, t_{j-1}]$ and O such that Eq. (6) is recovered.

Analogous to Eq. (7), we naturally define multi-point contour-ordered correlation functions, such as the two-point function $\frac{1}{Z} \operatorname{Tr} T_{\mathcal{C}}\, e^{-i\int_{\mathcal{C}} dt H(t)} A(t)B(t')$. In short, we will use the notation

$$\frac{1}{Z} \operatorname{Tr} T_{\mathcal{C}}\, e^{-i\int_{\mathcal{C}} dt H(t)} A(t)B(t')\cdots = \langle T_{\mathcal{C}} \hat{A}(t)\hat{B}(t')\cdots \rangle_H, \tag{10}$$

where $\langle \cdots \rangle_H = \frac{1}{Z} \operatorname{Tr} e^{-\beta H(0)} \cdots$ is the initial state expectation value, and an operator $\hat{O}(t)$ (with a hat) is understood in the Heisenberg picture, $\hat{O}(t) = \mathcal{U}(0,t) O \mathcal{U}(t,0)$. When all time arguments are on the imaginary branch of $\mathcal{C}$, contour-ordered correlation functions are identical to the imaginary-time correlation functions considered in the Matsubara formalism

$$\big\langle T_{\mathcal{C}} \hat{A}(-i\tau)\hat{B}(-i\tau')\cdots \big\rangle_H = \frac{1}{Z} \operatorname{Tr} T_\tau e^{-i\int_0^\beta d\bar{\tau} H(\bar{\tau})} A(\tau)B(\tau'). \tag{11}$$

Keldysh action

The discrete time formulation (9) shows that contour-ordered expectation values can be represented as a path integral, in full in analogy to imaginary-time ordered expectation values. In particular, for a normal-ordered Hamiltonian $H[c^\dagger, c]$ in terms of creation and annihilation operators c and $c^\dagger$ (suppressing for simplicity single-particle labels for spin, orbital, momentum), the coherent state path integral for the partition function (or rather, any generating function for contour-ordered expectation values) is given by

$$Z = \mathrm{Tr}\, T_{\mathcal{C}}\, e^{-i\int_{\mathcal{C}} dt H(t)} = \int \mathcal{D}[\bar{c}, c] e^{iS[\bar{c}(t), c(t)]}, \quad S = \int_{\mathcal{C}} dt \Big(\bar{c}(t) i\partial_t c(t) - H[\bar{c}, c] \Big), \tag{12}$$

with anti-periodic or periodic boundary conditions

$$c(0_+) = \pm c(-i\beta) \tag{13}$$

for bosons or fermions, respectively. This expression is understood in the usual way as the $N \to \infty$ continuum limit of the path integral on a discretized time contour with timesteps $t_0 = 0_+, ..., t_N = -i\beta$, and action

$$S_N = \sum_{n=1}^{N} \delta t_n \Big(i\bar{c}_n \frac{\bar{c}_n - c_{n-1}}{\delta t_n} - H[\bar{c}_n, c_{n-1}] \Big), \quad c_n \equiv c(t_n), \;\; \delta t_n = t_n - t_{n-1}. \tag{14}$$

One should check that the exponent iS reduces to the usual imaginary time action

$$iS = -\int_0^\beta d\tau \left(\bar{c}(\tau) \partial_\tau c(\tau) + H[\bar{c}(\tau), c(\tau)] \right) \tag{15}$$

when $t = -i\tau$ is restricted to the vertical branch of $\mathcal{C}$.
With the action (12), contour-ordered expectation values have a path integral representation

$$\mathrm{Tr}\, T_{\mathcal{C}}\, e^{-i\int_{\mathcal{C}} d\bar{t} H(\bar{t})} A(t) B(t') \cdots = \int \mathcal{D}[\bar{c}, c] e^{iS} A(t) B(t') \cdots, \tag{16}$$

where on the right-hand side operators $O(t) \equiv O[\bar{c}(t), c(t)]$ are understood in their coherent state representation. In the following, we will use the notation

$$\big\langle A(t) B(t') \cdots \big\rangle_S = \frac{1}{Z} \int \mathcal{D}[\bar{c}, c] e^{iS} A(t) B(t') \cdots \tag{17}$$

for contour-ordered expectation values related to an action S.
It should be stressed that in spite of the imaginary contribution from the real-time branches of $\mathcal{C}$, the path integral is convergent for both bosons and fermions. For example, the action $iS = i\int_{\mathcal{C}} dt\, \bar{c}(t)(i\partial_t - \epsilon)c(t)$ for a single bosonic degree of freedom ($H = \epsilon c^\dagger c$) defines a convergent Gaussian integral, other than the path integral for a pure real-time path which would be marginally convergent. With this, field theoretical techniques like the formulation of effective actions and the Hubbard Stratonovich decoupling, as well as Wick's theorem and the derivation of perturbation theory carry over from the imaginary-time Matsubara formalism to the Keldysh formalism on the L-shaped contour $\mathcal{C}$ by a simple replacement of the time variable.

2.2 Contour-ordered Green functions

Definition and relation to other representations

The most important two-point correlation function for the formulation of many-body methods is the Green function

$$G_{jj'}(t,t') = -i\big\langle c_j(t)\bar{c}_{j'}(t')\big\rangle_S = -i\big\langle T_{\mathcal{C}}\,\hat{c}_j(t)\hat{c}^\dagger_{j'}(t')\big\rangle_H. \tag{18}$$

Here j denote single particle labels, such as orbital, spin, and lattice site. The contour-ordered Green function does not only naturally appear in the context of diagrammatic perturbation theory, but it also contains all information on experimentally accessible single-particle observables. Before formulating many-body theory, we therefore explain how to relate the contour-ordered Green functions to the Green functions which are conventionally used for the description of systems in equilibrium.
(i) When both time arguments are on the vertical branch, we have

$$G_{j,j'}(-i\tau,-i\tau') = iG^M_{j,j'}(\tau-\tau'), \tag{19}$$

where $G^M_{j,j'}(\tau-\tau') = -\big\langle T_\tau\hat{c}_j(\tau)\hat{c}^\dagger_{j'}(\tau')\big\rangle_H$ is the imaginary time-ordered Matsubara Green function. This relation will be in particular important below to relate expressions in the Matsubara and Keldysh formalism. (ii) When one time argument is on the lower and one the other on the upper real-time contour, the contour ordering implies a fixed operator ordering. The two possible orderings are

$$G_{j,j'}(t_-,t'_+) = -i\left\langle c_j(t)c^\dagger_{j'}(t')\right\rangle \equiv G^>_{j,j'}(t,t'), \tag{20}$$
$$G_{j,j'}(t_+,t'_-) = -i\xi\big\langle c^\dagger_{j'}(t')c_j(t)\big\rangle \equiv G^<_{j,j'}(t,t'), \tag{21}$$

with $\xi = 1$ ($\xi = -1$) for Bosons (Fermions). These two functions therefore represent the propagation of an additional particle ($G^>$) or a hole ($G^<$) in the time-evolving system. Finally, (iii), of relevance below are the retarded and advanced Greens functions

$$G^R_{j,j'}(t,t') = \Theta(t-t')\big(G^>_{j,j'}(t,t') - G^<_{j,j'}(t,t')\big), \tag{22}$$
$$G^A_{j,j'}(t,t') = \Theta(t'-t)\big(G^<_{j,j'}(t,t') - G^>_{j,j'}(t,t')\big). \tag{23}$$

Spectroscopic interpretation

The Green functions $G^>$ and $G^<$ have a direct interpretation in terms of spectroscopic probes that add or remove electrons, such as tunnelling experiments and (inverse) time-resolved photoemission spectroscopy [23]. In an idealized description of such an experiment, we couple a probe orbital f to a given orbital j of the system, by adding the term $H' = s(t-t_p)e^{i\omega(t-t_p)}f^\dagger c_j + h.c.$ to the Hamiltonian, where the function $s(t-t_p)e^{i\omega(t-t_p)}$ is a time-dependent probe field with probe frequency ω and probe envelope $s(t-t_p)$ centered around some probe time t_p. For electron addition (removal) the probe orbital is assumed to be filled (empty) at time $t = -\infty$, and

the signal $I^>$ ($I^<$) is given by the change $\left|\langle f^\dagger f\rangle_{t=\infty} - \langle f^\dagger f\rangle_{t=-\infty}\right|$ after and before the probe. Straightforward time-dependent perturbation theory leads to the expression

$$I_{jj}^{>(<)}(\omega, t_p) = \int dt\, dt'\; e^{i\omega(t-t')}(\pm i) G_{j,j}^{>(<)}(t_p+t, t_p+t')\; s(t)s(t')^* + \mathcal{O}(s^4). \tag{24}$$

The upper (lower) sign refers to electron addition (removal); Eq. (24) is stated for fermions. This equation will be used below for the interpretation of non-equilibrium Green functions within a spectral representation.

Relation to equilibrium Green functions

In equilibrium, translational invariance in time implies that real-time propagators $X(t,t')$ depend only on the time-difference, and can be represented using the Fourier transform $X(\omega) = \int dt\, e^{i\omega t} X(t,0)$. Within the spectroscopic interpretation with an infinitely long probe pulse ($s(t) = $ const.), Eq. (24) gives $I_j^{>(<)}(\omega) \propto \pm i G_{jj}^{>(<)}(\omega)$, so that the electron and hole propagator can be interpreted in terms of the electron addition and removal spectrum, respectively. A straightforward expansion in (many-body) energy eigenstates (Lehmann representation) shows that the Green functions (20) and (21) are related to a single spectral density $A_{j,j'}(\omega) = -\frac{1}{\pi}\operatorname{Im} G^R_{j,j'}(\omega+i0)$ and the Fermi function $f(\omega)$ (again, the relations are stated for fermions)

$$G^>_{j,j'}(\omega) = \quad 2\pi i A_{j,j'}(\omega) f(-\omega), \tag{25}$$

$$G^<_{j,j'}(\omega) = -2\pi i A_{j,j'}(\omega) f(\quad \omega). \tag{26}$$

The electron removal spectrum is therefore given by the spectral density $A(\omega)$ multiplied with an occupation function $f(\omega)$ that gives the probability to find a state at ω to be occupied, while the electron addition spectrum is given by the same spectrum and the probability to find the state unoccupied, $f(-\omega) = 1 - f(\omega)$. It should be emphasized that this relation holds for any system in thermal equilibrium, also an interacting one. The distribution function $f(\omega)$ is entirely universal, i.e., it does not depend on any details of the Hamiltonian but only on temperature. This universal relation is analogous to the fluctuation-dissipation theorem, which gives a universal relation between response functions and time-dependent autocorrelation functions which is valid for any system in thermal equilibrium.

Moreover, the Lehmann representation expansion shows that the spectral function is related to the Matsubara Green function by the analytical relation

$$G^M_{j,j'}(\tau) = -\int d\omega A_{j,j'}(\omega) e^{-\omega\tau} f(-\omega). \tag{27}$$

This highlights how, in equilibrium, it is in principle sufficient to solve the system on the imaginary branch of the contour. The knowledge of $G(\tau)$ would suffice to determine the spectrum, so that the equilibrium theory is complete in terms of the imaginary time propagators. In practice, however, extracting real frequency information from imaginary time Green functions is an ill-conditioned problem (analytical continuation).

Green functions in a time-evolving state: Wigner representation

In a time-evolving state, time-translational invariance is lost, so that both spectral and occupation functions depend on two time-arguments separately. It is still often convenient to introduce a partial Fourier representation: A symmetric choice is the Wigner transform for a function $X(t,t')$, with average time $t_{av} = (t+t')/2$ and a relative time $t_{\rm rel} = t-t'$, and a Fourier transform with respect to $t_{\rm rel}$,

$$X(t_{av},\omega) = \int dt_{\rm rel}\; e^{i\omega t_{\rm rel}}\, X(t_{av}+t_{\rm rel}/2, t_{av}-t_{\rm rel}/2). \tag{28}$$

For example, the Wigner transforms $G^{<,>}(t,\omega)$ are then naturally related to time-resolved electron addition and removal experiments: With a Gaussian probe profile $S(t) = \exp(-t^2/2\tau^2)$ with duration τ, Eq. (24) gives

$$I_j^{>(<)}(\omega,t) \propto \int d\omega'\, dt'\; (\pm i) G_{jj}^{>(<)}(t+t',\omega+\omega')\; e^{-t'^2/\tau^2} e^{-\omega'^2\tau^2}, \tag{29}$$

i.e., an average of $G_{jj}^{>(<)}(t,\omega)$ over a window of width $\delta t = \tau$ in time and $\delta\omega = 1/\tau$ in frequency which satisfies energy-time uncertainty.[1]
In analogy to Eqs. (25) and (26), we can parametrize $G^{>(<)}(t,\omega)$ in terms of a time-dependent spectral function and a time-dependent occupation function

$$G^{<}(\omega,t) = \quad 2\pi i A(\omega,t)\; F(\omega,t), \tag{30}$$

$$G^{>}(\omega,t) = -2\pi i A(\omega,t)\big(1-F(\omega,t)\big), \tag{31}$$

omitting orbital indices for simplicity (A and F are matrices in orbital space). This representation emphasizes that the real-time Keldysh formalism provides a set of equations which describe the joint evolution of the spectral and distribution functions, as outlined in the introduction. This fact can also be turned into an approximate time-evolution scheme in terms of a quantum Boltzmann equation [24] which is an approximate equation of motion for a time-dependent occupation function, supplemented with certain approximations for the spectrum. One should note, however, that while $\pm iG^{>(<)}(t,\omega)$ is real (hermitian), it is not necessarily positive and cannot directly be interpreted in terms of a phase space probability in time and frequency. Only after averaging over an energy-time uncertainty window we obtain a positive quantity, see Eq. (29) above. This is analogous to the Wigner phase space density $W(x,p)$ as function of position and momentum, which becomes a phase space probability distribution only after suitably averaging over the conjugate variables x and p. Although the Wigner representation is often convenient to represent the time evolution, for numerical evaluation the (t,t')

[1] Note that this does not mean that $G(t,t')$ would be measurable only up to time-frequency uncertainty. Instead, Eq. (24) shows that in principle the full time dependence can be retrieved from experiment. For example, to measure $G^<(t,t')$ in a given time window, we choose an orthonormal basis $\phi_n(t)$ for time-dependent functions in that interval, and expand $-iG^<(t,t') = \sum_{n,n'} \phi_n^*(t) g_{n,n'} \phi_{n'}(t')$. The matrix $g_{n,n'}$ is hermitian and positive definite. A probe pulse $S(t) = \phi_n(t)$ then measures the diagonal components, $I^< = g_{n,n}$. A probe pulse $S(t) = \phi_n(t) + e^{i\varphi}\phi_m(t)$ gives $I^< = g_{n,n} + g_{m,m} + e^{-i\varphi} g_{n,m} + e^{i\varphi} g_{n,m}$, so that off-diagonal components $g_{n,m}$ can be obtained by scanning the phase difference φ [25].

representation is therefore often more suitable, because it allows for a causal time-propagation algorithm even on short timescales where A and F cannot be understood as positive distribution functions.

Causal property of contour-ordered functions

Finally, we note an important property of contour-ordered correlation functions which will be used below. The values of the contour-ordered function $G(t,t')$ with t and t' on different branches of $\mathcal{C}$ are not all independent, because the largest real-time argument can be shifted between the upper to the lower contour branch. For example, for $t' < t$,

$$G(t_+,t'_+) = \frac{1}{Z}\,\mathrm{Tr}\, e^{-\beta H(0)} \underbrace{\mathcal{U}(0,t)\mathcal{U}(t,t_{\max})}_{\mathcal{C}_-}\underbrace{\mathcal{U}(t_{\max},t)c\mathcal{U}(t,t')c^\dagger\mathcal{U}(t',0)}_{\mathcal{C}_+} = G(t_-,t'_+). \quad (32)$$

The brackets indicate the part of the contour-ordered operator $T_\mathcal{C} e^{-i\int_\mathcal{C} dt H(t)}$ along the upper and lower branch, respectively. Because the time-evolution between t and $t_{\max}$ along the upper and lower branch cancel, c can be shifted between the two branches. The redundancy which follows from Eq. (32) can be used to represent the contour-ordered Green functions in terms of fewer components; in particular, real time components can always be represented in terms of $G^<$ and $G^>$, hence the knowledge of the contour-ordered Green function is precisely equivalent to the knowledge of time-dependent spectral and distribution functions.

2.3 Perturbation theory

Equation of motion and inverse Green functions

The action (12) for the noninteracting Hamiltonian $H(t) = \epsilon(t)c^\dagger c$ can be written as a quadratic form $S = \int dtdt'\,\bar{c}(t)\delta_\mathcal{C}(t,t')(i\partial_t - \epsilon)c(t')$. Here $\delta_\mathcal{C}(t,t')$ is the delta-function consistent with the contour integral, i.e., $\int_\mathcal{C} dt'\,\delta_\mathcal{C}(t,t')g(t') = g(t)$ for any function $g(t)$ on $\mathcal{C}$. This quadratic action is to be understood as the continuum limit of a discrete form $S = \sum_{a,a'}\bar{c}_a A_{aa'}c_{a'}$ where a, a' label all orbital and discrete time indices. Gaussian integration for the discrete action yields the moments

$$\langle c_a\bar{c}_{a'}\rangle_S = \frac{1}{Z}\int \mathcal{D}[\bar{c},c]e^{iS}c_a\bar{c}_{a'} = \frac{1}{Z}\int \mathcal{D}[\bar{c},c]e^{-\sum_{b,b'}\bar{c}_b(-iA_{bb'})c_{b'}}c_a\bar{c}_{a'} = (iA^{-1})_{a,a'}. \quad (33)$$

i.e., the Greens function $G_{aa'} = -i\langle c_a\bar{c}_{a'}\rangle_S$ and A are inverse matrices in time. Reinstating the continuum limit, the equation $A\cdot G = 1$ yields the equation of motion for the free Green function G,

$$\int_\mathcal{C} d\bar{t}\,\delta_\mathcal{C}(t,\bar{t})(i\partial_{\bar{t}} - \epsilon)G(\bar{t},t') = \big(i\partial_t - \epsilon(t)\big)G(t,t') = \delta_\mathcal{C}(t,t'). \quad (34)$$

In the derivation of this equation one should note that in contrast to the inverse of the discrete matrix A, the differential equation (34) does not have a unique solution unless a proper boundary condition is specified. This boundary condition is provided by the relation

$$G(0_+,t) = \xi G(-i\beta,t), \quad G(t,0_+) = \xi G(t,-i\beta), \quad (35)$$

with the Bose (Fermi) sign ξ, which follows from the (anti)-periodic boundary condition (13) of c and $\bar{c}$ in the path integral.
From now on we use a continuum notation assuming that all operations take place within the space of (anti)-periodic functions. Multiplication of two contour functions corresponds to convolution along $\mathcal{C}$,

$$[A * B](t,t') = \int_{\mathcal{C}} d\bar{t}\, A(t,\bar{t})B(\bar{t},t'), \tag{36}$$

and the inverse $A^{-1}(t,t')$ of a function $A(t,t')$ is understood as the differential or integral equation $\int_{\mathcal{C}} d\bar{t}\, A^{-1}(t,\bar{t})A(\bar{t},t') = \int_{\mathcal{C}} d\bar{t}\, A(t,\bar{t})A^{-1}(\bar{t},t') = \delta_{\mathcal{C}}(t,t')$ with the boundary condition (35) (additional matrix multiplication in orbital indices implied).

Wick's theorem

Wick's theorem is a consequence of Gaussian integrals, and it therefore holds for contour-ordered functions as well as for imaginary time-ordered functions: For a quadratic action $iS_0 = -\sum_{a,a'} \bar{c}_a(-iA_{aa'})c_{a'}$, the n-point expectation values factorize in two-point functions,

$$\langle c_1 \cdots c_n \bar{c}_{n'} \cdots \bar{c}_{1'} \rangle_{S_0} = \sum_{\pi} \xi^{\pi} \langle c_1 \bar{c}_{\pi(1)'} \rangle_{S_0} \cdots \langle c_n \bar{c}_{\pi(n)'} \rangle_{S_0}. \tag{37}$$

where π runs over all permutations of the numbers $(1,...,n)$, and ξ^{π} is the sign of the permutation for fermions and 1 for bosons, i.e., the right hand side of the expression is the determinant (permanent) of the matrix $M_{ij} = \langle c_j \bar{c}_{j'} \rangle_S$ for fermions (bosons). Wick's theorem therefore directly implies a factorization of contour-ordered correlation functions for a noninteracting Hamiltonian H_0,

$$(-i)^n \big\langle T_{\mathcal{C}} \hat{c}(t_1) \cdots \hat{c}(t_n) \hat{c}^{\dagger}(t'_n) \cdots \hat{c}^{\dagger}(t'_1) \big\rangle_{H_0} = \sum_{\pi} \xi^{\pi} G_0(t_1, t'_{\pi(1)}) \cdots G_0(t_n, t'_{\pi(n)}) \tag{38}$$

in terms of the Green function $G_0(t,t') = -i\big\langle T_{\mathcal{C}} \hat{c}(t) \hat{c}^{\dagger}(t') \big\rangle_{H_0}$.
For illustration, let use the factorization of contour-ordered correlation functions to analyze the function

$$\chi^R(t,t') = -i\Theta(t-t') \left\langle [\hat{O}(t), \hat{O}(t')] \right\rangle_H, \tag{39}$$

which gives the response of the operator O to a time dependent field coupling to O (Kubo relation). In the Matsubara formalism, the response is obtained from the analytical continuation of the imaginary-time ordered correlation function $\chi(\tau) = -\big(\big\langle T_\tau \hat{O}(\tau)\hat{O}(0) \big\rangle - \langle O \rangle^2\big)$; taking a noninteracting fermionic system $H = \sum_a \epsilon_a c_a^{\dagger} c_a$ and a single particle observable $O = \sum_{ab} o_{ab} c_a^{\dagger} c_b$, one would, after some algebra, obtain the convolution of the unoccupied density of states $A_a^{>}(\omega) = A_a(\omega) f(-\omega)$ and the occupied density of states $A_a^{<}(\omega) = A_a(\omega) f(\omega)$,

$$-\frac{1}{\pi} \operatorname{Im} \chi^R(\Omega^+) = \sum_{a,b} |o_{ab}|^2 \int d\omega \left(A_b^{>}(\omega+\Omega) A_a^{<}(\omega) - A_b^{>}(\omega-\Omega) A_a^{<}(\omega) \right). \tag{40}$$

For $\Omega > 0$, the two parts of the expression naturally describe energy absorption and emission when going from an occupied state a to and unoccupied state b. The same expression can be obtained in a relatively straightforward manner from the Keldysh formalism. We start from the contour-ordered correlation function $\chi(t,t') = -i\big(\big\langle T_{\mathcal{C}}\hat{O}(t)\hat{O}(t')\big\rangle - \big\langle\hat{O}(t)\big\rangle\big\langle\hat{O}(t')\big\rangle\big)$, which is related to the response function by

$$\chi^R(t,t') = \Theta(t{-}t')\,\big(\chi(t_-,t'_+) - \chi(t_+,t'_-)\big). \tag{41}$$

Application of Wick's theorem for general contour arguments (t,t') directly gives

$$\chi(t,t') = -i\sum_{ab,cd} o_{ab}o_{cd}\,\big\langle T_{\mathcal{C}}\hat{c}^\dagger_a(t)\hat{c}_d(t')\big\rangle_{H_0}\big\langle T_{\mathcal{C}}\hat{c}_b(t)\hat{c}^\dagger_c(t')\big\rangle_{H_0} = -i\sum_{ab}|o_{ab}|^2\,G_{aa}(t,t')\,G_{bb}(t',t).$$

where in the second step we used that $G_{ab} = \delta_{ab}G_{aa}$. Using $G(t_+,t'_-) = G^<(t,t')$ and $G(t_-,t'_+) = G^>(t,t')$, we can read off

$$\chi(t_-,t'_+) = -i\sum_{ab}|o_{ab}|^2\,G^>_{aa}(t,t')\,G^<_{bb}(t',t)\,,\quad \chi(t_+,t'_-) = -i\sum_{ab}|o_{ab}|^2\,G^<_{aa}(t,t')\,G^>_{bb}(t',t),$$

after which the spectral representation (30) and (31) directly yields Eq. (40) by inverse Fourier transform. This exercise should highlight how working with contour-ordered Green functions in equilibrium is equivalent to and working with imaginary time Green functions and doing an analytical continuation.

Diagrammatic perturbation theory

Because Wick's theorem applies for contour-ordered correlation functions as well as for imaginary time-ordered functions, the construction of diagrammatic perturbation theory does not depend on the time contour, and is formally the same for Matsubara Green functions and contour-ordered Green functions. Green functions are represented in terms of connected diagrams G representing products of the noninteracting Green function G_0 and the interaction V. Because the Keldysh formalism is obtained from the Matsubara formalism by just replacing the time contour, one can translate a diagram for $G^M(\tau{-}\tau')$ in terms of the noninteracting Green function $G_0^M(\tau)$ and the interaction $V(\tau)$ to the Keldysh formalism by using the following rules:

(42)

(1) For all correlation functions ($X \equiv G,\ G_0,\ V$), replace $X^M(\tau_i{-}\tau_j)$ by $-iX(t_i,t_j)$, where the arguments represent either external arguments τ and τ' or internal arguments, which are later integrated over [cf. Eq. (19)].

(2) Replace internal integrals $\displaystyle\int_0^\beta d\tau_j$ by $\displaystyle i\int_{\mathcal{C}} dt_j$.

(3) Replace $\delta(\tau{-}\tau')$ by the contour delta function $-i\delta_{\mathcal{C}}(t,t')$.

For example, let us illustrate these rules for the retarded interaction (omitting spin and site indices for simplicity)

$$S_V^M = \int_0^\beta d\tau d\tau'\,\bar{c}(\tau^+)c(\tau)\,V(\tau{-}\tau')\,\bar{c}(\tau'^+)c(\tau'), \tag{43}$$

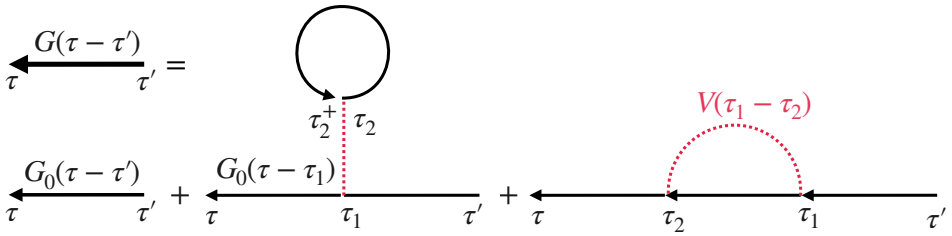

Fig. 2: *Leading diagrams for the expansion of the Green function* $G(\tau) = -\langle T_\tau c(\tau) c^\dagger(0)\rangle$ *in terms of the interaction terms* (43)*, corresponding to the Hartree (left diagram) and Fock (right diagram) self energy.*

in the imaginary-time formalism, where the superscript $+$ means that the time argument is infinitesimally later. The last two diagrams in Fig. 2, obtained by expanding $e^{-S_V^M}$ to leading order in the expression $G(\tau) = -\langle T_\tau c(\tau) c^\dagger\rangle$, reads in the Matsubara formalism

$$\begin{aligned} G(\tau-\tau') = &- \int d\tau_1 d\tau_2 \; G_0(\tau-\tau_1)\, G_0(\tau_1-\tau_2)\, G_0(\tau_2-\tau')\, V(\tau_1-\tau_2) \\ &+ \int d\tau_1 d\tau_2 \; G_0(\tau-\tau_1)\, G_0(\tau_2-\tau_2^+)\, G_0(\tau_1-\tau')\, V(\tau_1-\tau_2), \end{aligned} \tag{44}$$

Hence in the Keldysh formalism we have

$$\begin{aligned} G(t,t') = &\, i \int_{\mathcal{C}} dt_1 dt_2 \; G_0(t,t_1) G_0(t_1,t_2) G_0(t_2,t') V(t_1,t_2) \\ &- i \int_{\mathcal{C}} dt_1 dt_2 \; G_0(t,t_1) G_0(t_2,t_2^+) G_0(t_1,t') V(t_1,t_2), \end{aligned}$$

where, using rules (i) and (ii) above, the overall sign is determined from a factor $(-i)$ on the left-hand side (one propagator) and a factor $(-i)^4 i^2$ (four propagators, two integrals) on the right-hand side. An instantaneous interaction is $V(\tau-\tau') = \delta(\tau-\tau')\, U$ is replaced by $-iV(t,t') = -i\delta_{\mathcal{C}}(t,t')\, U(t)$ using rules (i) and (iii).

As in the Matsubara formalism, we introduce the self-energy $\Sigma(t,t')$, which is the sum of all one-particle irreducible diagrams without external Green functions legs, from which the Green function is obtained by the Dyson equation. The latter is replaced from the Matsubara contour,

$$G(\tau-\tau') = G_0(\tau-\tau') + \int_0^\beta d\tau_1 d\tau_2\, G_0(\tau-\tau_1)\, \Sigma(\tau_1-\tau_2)\, G(\tau_2-\tau') \tag{45}$$

using again rules (i) and (ii), to the integral equation on $\mathcal{C}$,

$$G(t,t') = G_0(t,t') + \int_{\mathcal{C}} dt_1 dt_2\, G_0(t,t_1)\, \Sigma(t_1,t_2)\, G(t_2,t'). \tag{46}$$

For example, the first order self energy (Hartree and Fock) can be read off Eq. (44),

$$\Sigma_H(\tau-\tau') = \delta(\tau-\tau') \int d\tau_1 V(\tau-\tau_1)\, G(\tau_1-\tau_1^+) \tag{47}$$

$$\Sigma_F(\tau-\tau') = -V(\tau-\tau')\, G(\tau,\tau'), \tag{48}$$

where in the first line the argument τ_1^+ is infinitesimally later than τ_1, so that $G(\tau_1-\tau_1^+) = \langle c^\dagger c\rangle \equiv n$ is the density. In the Keldysh formalism, the above rules give

$$\Sigma_H(t,t') = -i\delta_{\mathcal{C}}(t,t')\int_{\mathcal{C}} dt_1 V(t,t_1)\, G(t_1,t_1^+) \tag{49}$$

$$\Sigma_F(t,t') = iV(t,t')\, G(t,t'). \tag{50}$$

In the first line, $-iG(t_1,t_1^+) = n(t)$ is again the density. For an instantaneous interaction $V(\tau-\tau') = \delta(\tau-\tau')\, U$, the Hartree diagram is thus $\Sigma_H(t,t') = \delta(t,t')\, Un(t)$. A more interesting exercise is to rewrite the contribution for a retarded interaction. In this case, for t on the real-branch of $\mathcal{C}$ the contour integral can be rewritten as

$$\int_{\mathcal{C}} dt_1 V(t,t_1)\,(-i)\, G(t_1,t_1^+) = \int_{\mathcal{C}} dt_1 V(t,t_1)\, n(t_1) = \int_{-\infty}^{\infty} dt_1 \big(V(t,t_{1,+})-V(t,t_{1,-})\big) n(t_1),$$

where we have shifted the imaginary branch of $\mathcal{C}$ to $t=-\infty$, and assumed that $V(t,t')$ decays sufficiently fast; in the last step, the contour integral is written explicitly in terms of integrals over the upper and lower branch, with opposite integration direction. Finally, using the causality property (32), which allows to shift the larger of the two arguments t and t_1 freely between the upper/lower contour, the integral is transformed to

$$\int dt_1 n(t_1)\,\Theta(t-t_1)\big(V(t_{1,+},t_-)-V(t_{1,-},t_+)\big) = \int dt_1 V^R(t,t_1)\, n(t_1). \tag{51}$$

The Hartree self energy is therefore given by

$$\Sigma_H(t,t') = \delta_{\mathcal{C}}(t,t')\int dt_1 V^R(t,t_1)\, n(t_1) \equiv \delta_{\mathcal{C}}(t,t')\, V_{\text{mf}}(t), \tag{52}$$

which is a time-dependent mean-field potential $V_{\text{mf}}(t)$; one can see that the retarded interaction is the response function that determines the mean-field potential at time t due to the density at time t_1.

Numerical solution of the Dyson equation

For a given self-energy, the Dyson equation (46) must be solved in order to obtain the Green function. Writing Eq. (46) in short as $G = G_0 + G_0 * \Sigma * G$, it can be reformulated in the form $G^{-1} = G_0^{-1} - \Sigma$, with the inverse operator in time as introduced below Eq. (36). For the noninteracting problem $H_0 = \sum_{ab} c_a^\dagger h_{ab}(t) c_b$, the inverse Green function is $G_0^{-1} = \delta_{\mathcal{C}}(t,t')\big(i\partial_t - h(t)\big)$ [cf. Eq. (34)], so that the Dyson equation can be formulated as an integral differential equation on $\mathcal{C}$,

$$\big(i\partial_t - h(t)\big)\, G(t,t') - \int_{\mathcal{C}} d\bar{t}\, \Sigma(t,\bar{t})\, G(\bar{t},t') = \delta_{\mathcal{C}}(t,t') \tag{53}$$

(omitting orbital and spin indices, i.e., G, h, Σ are understood as matrices in orbital space). Equation (53) and the equivalent Eq. (46) are integral and integro-differential equations on $\mathcal{C}$, which in most cases must be solved numerically (Kadanoff-Baym equations). It is important

to note that one can obtain the solution in a time-stepping manner: With an equidistant time grid ($t_n = n\delta t$), let us denote the nth timeslice of the two-time function $X(t,t')$ to include all elements where one argument is $n\delta t$ and the other is either $m\delta t$ with $m \leq n$ or on the imaginary time branch; timeslice $n = -1$ is simply the Matsubara component of X (both time arguments on the imaginary time branch). Causality then implies that G on timeslice n can be computed from G on all timeslices $m < n$ and Σ on all timeslices $m \leq n$ as an input. Moreover, the self-energy $\Sigma[G]$ must be a causal functional of G, which implies that Σ on timeslice n can be evaluated in terms of G (or G_0) on timeslices $m \leq n$. Hence the typical evolution algorithm will proceed in two steps:

(1) Initial state simulation: Solve the problem on the imaginary time axis, in order to determine the Matsubara components of Σ and G.

(2) Timestepping: For each $n \geq 0$, do the following: (i) Extrapolate Σ from timeslice $n-1$ to timeslice n. (ii) Compute G on timesline n by solving the Dyson equation. (iii) Compute Σ on timeslice n using G on timesline $m \leq n$. Iterate (ii) and (iii) until convergence.

Having in mind that G basically contains the information on spectral and distribution function, one can again see that the Keldysh formalism provides a joint equation of motion for spectral and distribution functions, which is nonlinear (because Σ is a nonlinear functional of G) and non-Markovian, i.e., the propagation depends on all the history. The actual implementation depends on the parametrization of the Green functions. Detailed implementations are described, e.g., in Refs. [26] and [20]. The latter is the basis for the open source code NESSi `http://www.nessi.tuxfamily.org`, which provides a high-order accurate solution of various integral equations on $\mathcal{C}$, as well as basic routines to construct diagrams from contour-ordered Green functions.

In spite of being just a linear equation, the solution of the Dyson equation can provide a severe numerical bottleneck, in particular for multi-orbital simulations. Determination of G for each element of a timeslice n requires a convolution integral over all previous times. Hence the numerical effort to solve the Dyson equation up to time n scales like $\mathcal{O}(n^3)$. More serious is the requirement to keep G and/or Σ at all previous timeslices in memory: For example, for a realistic simulation with $L = 10$ bands in an energy window of $10\,\mathrm{eV}$ over a time window of $1\,\mathrm{ps}$=$1000\,\mathrm{fs}$, we can expect that the timestep δt should resolve the inverse of the largest energy scale, $\delta t \ll \hbar/10\,\mathrm{eV} \approx 0.1\,\mathrm{fs}$, so that the simulation would extend over at least $n = 10^4$ timesteps (probably more). With each element $G(t,t')$ being an $L\times L$ matrix in orbital space, this corresponds to 10^{10} complex numbers or, more than $100\,\mathrm{GB}$. As one of such objects must be kept for each momentum in a suitably discretized Brillouin zone, realistic materials simulations would quickly reach the limit of current day computational capabilities.

Clearly, the equidistant discretization is far from optimal, and there are several directions discussed in the present literature to overcome these limitations. A simple possibility is to implement a systematic truncation of the memory kernel $\Sigma(t,t')$ within the time-stepping procedure [27]. In this way, simulations up to $n = 10^6$ timeslices could be performed within DMFT

simulations [28,29] for certain parameters. In this case, the numerical effort scales linearly with n, and the memory is constant. Another promising route is to explore different compact representations of the two-time functions, such as hierarchical storage formats [30]. Beyond that, also approximate solutions of the integral equations, such as the Generalized Kadanoff-Baym Ansatz [31] or Quantum Boltzmann equations [32, 33] have the potential to extend simulations over a large number of timesteps n at a linear cost $\mathcal{O}(n^1)$ in computation and a constant cost $\mathcal{O}(n^0)$ in memory.

3 Non-equilibrium DMFT and beyond

3.1 Non-equilibrium DMFT

Non-equilibrium DMFT formalism

DMFT approximates only the spatial correlations in a mean-field manner, but accurately treats local temporal fluctuations. The main approximation is the locality of the self-energy, which becomes exact in the limit of infinite coordination number [34]. The formulation of DMFT within the Keldysh and the Matsubara framework differs only by the choice of the time contour, and all arguments regarding the derivation of DMFT, such as the cavity method [11] and power counting arguments for the locality of the self-energy, can be transferred one-to-one from imaginary time to $\mathcal{C}$. We therefore only briefly summarize the formalism. For clarity, the DMFT equations in this section are all stated for the single-band Hubbard model in the spin-symmetric phase; orbital indices can easily be added.
With a spatially local self energy $\Sigma_{ij} = \delta_{ij}\Sigma_{jj}$, lattice Green functions are obtained by solving the Dyson equation

$$G^{-1}_{jj'}(t,t') = \big(i\partial_t + \mu\big)\delta_{\mathcal{C}}(t,t')\delta_{jj'} - \delta_{jj'}\Sigma_{jj}(t,t') - \delta_{\mathcal{C}}(t,t')v_{ij}(t), \tag{54}$$

where $v_{ij}(t)$ are the hopping matrix elements, which contain the external laser fields. To obtain a best local approximation to the self-energy, one can imagine to start from the skeleton expansion $\hat{\Sigma}[G]$ of the self energy, i.e., a diagrammatic expansion in terms of the fully dressed propagator G, and then restrict the expansion for Σ_{jj} to the terms which contain only the local propagator G_{jj}, but are otherwise summed up to all orders in the interaction. Due to the locality of the interaction, these local contributions to the skeleton expansion can be generated by solving an impurity model with a single interacting site and an arbitrary noninteracting environment (bath). Because the functional form of the skeleton expansion does not depend on the noninteracting part of the action, the functional dependence of the impurity self-energy $\Sigma_{\text{imp}}[G_{\text{imp}}]$ on the impurity Green function is the same as the functional dependence of the local lattice self energy $\Sigma_{jj}[G_{jj}]$ on the local Green function. Hence, the impurity self-energy serves as an approximation for the lattice self-energy,

$$\Sigma_{jj'}(t,t') = \delta_{jj'}\Sigma_{\text{imp}}(t,t'), \tag{55}$$

as long as the bath is designed such that the self-consistency condition

$$G_{\text{imp}}(t,t') \stackrel{!}{=} G_{jj}(t,t'). \tag{56}$$

is satisfied. (For simplicity of notation, we also assume translational invariance in space.) For this construction, the impurity model must have the same local interaction as the lattice model, and a general quadratic contribution to the action,

$$S_{\text{imp}} = \int_{\mathcal{C}} dt dt' \Big(\sum_{\sigma} \bar{c}_\sigma(t) \mathcal{G}_\sigma^{-1}(t,t') c_\sigma(t) - U(t)\, \bar{c}_\uparrow(t) c_\uparrow(t) \bar{c}_\downarrow(t) c_\downarrow(t) \delta_{\mathcal{C}}(t,t') \Big), \tag{57}$$

$$\mathcal{G}^{-1}(t,t') = \big(i\partial_t + \mu\big)\delta_{\mathcal{C}}(t,t') - \Delta(t,t'), \tag{58}$$

which describes one site of the lattice embedded in an environment with hybridization function $\Delta(t,t')$. This is the action of a time-dependent Anderson Impurity Hamiltonian. From the action one obtains the interacting impurity Green function

$$G_{\text{imp}}(t,t') = -i\big\langle c(t)\bar{c}(t')\big\rangle_{S_{\text{imp}}}, \tag{59}$$

and the impurity self-energy is set by the impurity Dyson equation

$$G_{\text{imp}}^{-1}(t,t') = \mathcal{G}^{-1}(t,t') - \Sigma_{\text{imp}}(t,t'). \tag{60}$$

Equations (54) through (60) provide the closed set of equations for non-equilibrium DMFT, and the auxiliary quantity $\Delta(t,t')$ can be eliminated when the local lattice Green function G_{jj} equals the corresponding impurity quantity.

The actual implementation of the self-consistency depends on the algorithm used to solve the impurity model. Keeping in mind that the self-consistent equations are integral equations in time, one should bring them to a form that is numerically most stable. For example, G^{-1} is an integral operator which has a singular contribution $\delta_C(t,t')i\partial_t$ on the time diagonal [cf. Eq. (34)], Eq. (60) cannot be directly solved for Σ_{imp} on a given time grid after G_{imp} has been calculated. Instead, one can e.g., extract the function $Z = (i\partial_t + \mu - \Sigma_{\text{imp}})^{-1}$ by solving the linear equation

$$G_{\text{imp}} = Z * (1 + \Delta * G_{\text{imp}}) \tag{61}$$

for Z (this equation is equivalent to (60) and (58)), and then use Z to solve Eq. (54) for the lattice Green function in its equivalent integral form $(1 - Z * v) * G = Z$.

3.2 Impurity solvers

The most challenging part of the DMFT equations is the solution of the auxiliary problem, i.e., the determination of the Green function (59) from the action (57) with a given hybridization function $\Delta(t,t')$. Like in equilibrium DMFT, the action (57) can be mapped to a single impurity Anderson impurity model (SIAM)

$$H_{\text{SIAM}} = U c_\uparrow^\dagger c_\uparrow c_\downarrow^\dagger c_\downarrow + \sum_{p,\sigma} \epsilon_{p,\sigma}\, a_{p\sigma}^\dagger a_{p\sigma} + \sum_{p,\sigma} \big(V_p(t) a_{p,\sigma}^\dagger c_\sigma + h.c. \big), \tag{62}$$

with time-dependent hybridization $V_p(t)$ to bath orbitals labelled by p. In fact, one can see that the hybridization function Δ_{SIAM} representing the discrete bath in the SIAM is given by

$$\Delta_{\text{SIAM}}(t,t') = \sum_p V_p(t) g_p(t,t') V_p^*(t'), \tag{63}$$

with the isolated Green function g_p of a single site of the bath [35]. Hence the parameters V_p can be determined by a simple fit of the analytical expression $\Delta_{\text{SIAM}}(t,t')$ to the hybridization obtained from the DMFT self-consistency. The most efficient way to make use of this discrete representation has been to compute the time-dependent Green functions using a many-body wave function $|\Psi(t)\rangle$ in a matrix product state (MPS) representation [36]. However, while a MPS representation is efficient for ground states which satisfy an area-law entanglement, the time-propagated state can often not be represented efficiently, leading to an exponential increase of computational resources with the simulated time. This has restricted simulations so far to relatively short times [37]. Moreover, it turns out to be necessary to increase the number of bath orbitals in the representation (63) for large time in order to ensure that $\Delta_{\text{SIAM}}(t,t')$ decays as a function of relative time, as required for a continuum bath. To ensure such a decay, one could couple the bath orbitals themselves to simple reservoirs that can be treated within a Lindblad equation. This would increase the computational cost, as it requires a propagation of the many-body density-matrix instead of the wave function, but it would allow to keep the number of auxiliary bath sites fixed for long time simulations. Such an open system representation for the non-equilibrium SIAM has been used so far only to solve DMFT for non-equilibrium steady states [38].

An alternative to the discrete bath representation are Quantum Monte Carlo (QMC) techniques, which can give numerically exact results in equilibrium [39]. A direct extension of QMC algorithms by extending the time contour from the imaginary to the L-shaped contour suffers from a severe phase problem and is restricted to very short times. There are interesting and fundamental problems related to in the short-time dynamics, such as dynamical phase transitions [40], but in order to study the photo-induced dynamics in most materials few hopping times are often not yet sufficient. More promising real-time QMC algorithms are formulated in the spirit of diagrammatic Monte Carlo methods, such as the so called inchworm algorithm [41] which samples the self-energy in the strong coupling expansion, or is vertex generalization, the recently proposed slime-mold algorithm [42]. So far the high numerical cost has prevented an application of these approaches within real-time DMFT simulations, but recent developments in particular towards non-equilibrium steady state DMFT promise that real-time Quantum Monte Carlo may soon be used to simulate the photo-induced dynamics of correlated solids.

Most applications of non-equilibrium DMFT to describe photo-induced dynamics in solids have been based on a perturbative solution of the impurity model, such as adaptations of the iterated perturbation theory [11], or alternatively a systematic expansion in $\Delta(t,t')$ [43]. In this so-called strong-coupling expansion one splits the action S into the local part $S_{at} = \int_{\mathcal{C}} dt H_{at}(t)$, with the atomic Hamiltonian H_{at} that contains the local interaction, and the time-nonlocal terms

S_{n-l}. The latter can have a very general form, such as

$$S_{n-l} = \sum_{\gamma} \int_{\mathcal{C}} dt_1 dt_2 \, \bar{\phi}_\gamma(t) \Delta_\gamma(t,t') \psi_\gamma(t'), \tag{64}$$

where γ sums over all hybridization and interaction channels, and ψ and $\bar{\phi}$ are general operators. In the single impurity Anderson model, e.g., $\gamma \equiv \sigma$, $\bar{\phi}_\gamma \equiv \bar{c}_\sigma$, $\psi_\gamma \equiv c_\sigma$, but the general formulation also allows for inter-orbital hybridizations in multi-band systems, anomalous hybridizations in superconducting systems, $\int_{\mathcal{C}} dt_1 dt_2 \big(c_\uparrow(t)\Delta_{cc}(t,t')c_\downarrow(t') + \bar{c}_\downarrow(t)\Delta_{\bar{c}\bar{c}}(t,t')\bar{c}_\uparrow(t')\big)$, retarded density-density interactions $\sum_{\sigma\sigma'} \int_{\mathcal{C}} dt_1 dt_2 \, n_\sigma(t) V_{\sigma,\sigma'}(t,t') n_\sigma(t')$ (here $\bar{\phi}_{\sigma,\sigma'} \equiv \bar{c}_\sigma c_\sigma$ and $\psi_{\sigma,\sigma'} \equiv \bar{c}_{\sigma'} c_{\sigma'}$), or electron-phonon interactions ($\psi = c_\sigma b, c_\sigma \bar{b}$ etc., acting in a local space of electrons and phonons). The strong-coupling expansion is expected to work well in the Mott phase, as it can be formulated for an arbitrary local part of the Hamiltonian, and it defines a conserving approximation (which respects conservation laws of energy and particle number also in the approximate solution of the time-evolution). In particular the lowest order (the so called non-crossing approximation, NCA) has been used extensively to study the dynamics of Mott-insulators within DMFT. The technical details of this expansion on the Keldysh contour are explained in Refs. [43] and [14] as well as in earlier notes of this lecture series [19].

3.3 Multi-band DMFT+GW

Extensions and Limitations of DMFT

The main limitation of DMFT is the local approximation to the self-energy. As in equilibrium DMFT, non-equilibrium variants have been formulated for both cluster extensions and diagrammatic extensions of DMFT. Cluster extensions are in particular important to keep short range correlations of spin and charge on the scale of few lattice sites, which can have a pronounced influence on the short time dynamics. For example, photo-excited carriers in a Mott insulator, as described in a one band Hubbard model, can loose kinetic energy on the timescale of few inverse hopping times due to the interaction with short-range antiferromagnetic order [44], i.e., the background of spin fluctuations serves a an efficient heat bath for the electronic quasiparticles, which can act much faster than the cooling of photo-excited carriers by coupling to phonons.

Another limitation of plain DMFT is the restriction to local interactions. An important consequence of non-local interactions in the solid is the feedback of the long-range Coulomb interactions on the parameters of the model Hamiltonians due to dynamical screening. For large excitation densities, or interactions involving many bands, one can expect a sizeable renormalization of the Hubbard U via screening, which may even close a Mott gap. The question of screening is also closely related to the determination of parameters for time-dependent models from ab-initio theory. The combination of a non-equilibrium Green function approach such as DMFT with time-dependent density functional theory encounters the double counting problem, which is even harder to solve out of equilibrium than in equilibrium simulations. An interesting perspective is therefore the combination of non-equilibrium GW with DMFT [45, 46], which

can be formulated in a consistent functional language. This formalism is presented in the next chapter, following mainly Ref. [47].

The GW+DMFT formalism

For simplicity we consider a system with several orbitals per unit cell, but only density-density interactions. The most general Hamiltonian is

$$H = \sum_{j,j'} \sum_{a,b} J_{j,a;j',a'} c^\dagger_{j,a} c_{j',a'} + \frac{1}{2} \sum_{j,j'} \sum_{a,a'} v_{j,a;j',a'} n_{j,a} n_{j',a'} \equiv H_0 + H_V \tag{65}$$

where j and j' label the unit cells, and a, a' are combined spin/orbital indices, J is the hopping matrix, and v the interaction. The action is therefore

$$S = \int d1 d2 \; \bar{c}(1)\, G_0^{-1}(1,2)\, c(2) - \frac{1}{2} \int d1 d2 \; n(1)\, V(1,2)\, n(2) \equiv S_0 + S_V, \tag{66}$$

where we have introduced a combined notation $1 \equiv (t_1, j_1, a_1)$ for time, space and orbital indices, with $\int d1 = \int_{\mathcal{C}} dt_1 \sum_{j_1,a_1}$, and $\delta(1,2) = \delta_{\mathcal{C}}(t_1,t_2)\delta_{j_1,j_2}\delta_{a_1,a_2}$, as well as the interaction matrix $V(1,2) = v_{j_1,a_1;j_2,a_2}\, \delta_{\mathcal{C}}(t_1,t_2)$, and the noninteracting Green function $G_0^{-1}(1,2) = (i\partial_{t_1} + \mu)\, \delta(1,2) - J(1,2)$. The first step is to decouple the interaction using a Hubbard-Stratonovich transformation using a real field $\varphi(1)$ and the Gaussian identity

$$e^{iS_V} = \frac{1}{Z_\varphi} \int \mathcal{D}[\varphi]\, e^{iS_\varphi} e^{-\int d1 \varphi(1) n(1)}, \quad S_\varphi = -\frac{1}{2} \int d1 d2 \; \varphi(1)\, V^{-1}(1,2)\, \varphi(2). \tag{67}$$

Here V^{-1} is inverse in site, orbital, and time, $\int d\bar{1}\, V^{-1}(1,\bar{1})\, V(\bar{1},1') = \delta(1,1')$. It is worthwhile to note that the Gaussian integral over φ in Eq. (67) is convergent: Using the rules Eq. (42), the action iS_φ reduces to $iS_\varphi = -\frac{1}{2}\int_0^\beta d\tau \sum_{j,a,j',a'} \varphi_{j,a}(\tau)(v^{-1})_{j,a;j',a'}\varphi_{j',a'}(\tau)$ on the Matsubara branch, which defines a convergent integral if the matrix v is positive definite (repulsive interaction).

After the Hubbard-Stratonovich decoupling, the system is described by electrons interacting with a fluctuating bosonic field φ, with the effective action

$$S_{\text{eff}}[c,\bar{c},\varphi] = S_\varphi[\varphi] + S_0[\bar{c},c] + i \int d1 \; \varphi(1)\, n(1), \tag{68}$$

in the sense that the partition function is $Z_{\text{eff}} = \int \mathcal{D}[\bar{c},c] \int \mathcal{D}[\varphi] e^{iS_{\text{eff}}[c,\bar{c},\varphi]}$. In the new representation, we then introduce the propagators W of the interaction as well as the electronic density correlation functions χ,

$$W(1,1') = \quad i\big\langle \varphi(1)\varphi(1') \big\rangle^{\text{con}}_{S_{\text{eff}}} \tag{69}$$

$$\chi(1,1') = -i\big\langle n(1)n(1') \big\rangle^{\text{con}}_{S_{\text{eff}}} \tag{70}$$

with the connected correlation function $\langle AB\rangle^{\text{con}} = \langle AB\rangle - \langle A\rangle\langle B\rangle$. The Hubbard Stratonovich transformation implies the exact relation

$$\langle \varphi(1) \rangle = i \int d\bar{1} \; V(1,\bar{1}) \langle n(\bar{1}) \rangle \equiv i V_{\text{mf}}(1) \tag{71}$$

$$W(1,1') = V(1,1') + \int d\bar{1} d\bar{2} \; V(1,\bar{1})\, \chi(\bar{1},\bar{2})\, V(\bar{2},1'), \tag{72}$$

which shows that $\varphi(1)$ takes the role of a fluctuating mean field, and its propagator W is the fully screened interaction. We can now use the action (68) and formulate the diagrammatic perturbation theory for the electronic (G) and bosonic (W) propagators in terms of the electron-boson interaction $e^{iS_{n-\varphi}} = e^{-\int d1 n(1)\varphi(1)}$, where the noninteracting propagators are the noninteracting Green function G_0 and the bare interaction V. We introduce self-energies $\Sigma[G,W]$ and $\Pi[G,W]$ for the electrons and bosons,

$$W^{-1} = V^{-1} - \Pi[W,G], \quad G^{-1} = G_0^{-1} - \Sigma[W,G]. \tag{73}$$

(Π is called the polarization function). The perturbation theory is formulated in terms of a self-consistent skeleton expansion, i.e., the propagators in the self-energies do not contain self-energy insertions. From the action, the lowest-order approximation would be [cf. Eqs. (47) and (48)]

$$\Sigma(1,1') = \quad iG(1,1')W(1,1') - i\langle\varphi(1)\rangle\,\delta(1,1') \equiv \Sigma_{GW}(1,1') - i\langle\varphi(1)\rangle\,\delta(1,1'), \tag{74}$$

$$\Pi(1,1') = -iG(1,1')\,G(1',1) \equiv \Pi_{GW}(1,1'). \tag{75}$$

The second term in Σ, together with the exact relation (71), is just the Hartree mean-field potential $-i\langle\varphi(1)\rangle\,\delta(1,1') = V_{\text{mf}}(1)\,\delta(1,1')$. The terms Σ_{GW} and Π_{GW} define the celebrated GW approximation, which was developed by Hedin [48]: In this approximation the electronic self-energy is expanded to leading order in the fully screened interaction, and the polarization is approximated by the Lindhard function expressed in terms of the renormalized electron propagators. While this approach is understood to be an accurate approximation in electronic structure calculations of weakly correlated materials, (superior to standard density functional approximations), it fails to describe the effect of strong local correlations, such as the Mott transition. To overcome this limitation, one can therefore combine the idea of DMFT with the GW approximation [45, 46]:

Let us assume that we can identify a certain subset C of orbitals which are considered to be strongly correlated, so that within that subset we would like to use a more accurate approximation for the self-energy and the polarization. In the spirit of DMFT, one can aim to add on top of the self-energy and polarization defined in Eqs. (74) and (75) a nonperturbative self-energy Σ_{corr} and polarization Π_{corr} which (i), act only on the correlated orbitals, (ii) are local in space, and (iii) are given by all contributions to the skeleton expansion which contain only the space-local propagators of the correlated manifold at the same site. In other words, we set

$$(\Sigma_{\text{corr}})_{j,a';j,a'}(t,t') = \begin{cases} \delta_{j,j'}\Sigma_{\text{loc,cor}}[G_{\text{loc,cor}}, W_{\text{loc,cor}}]_{a';a'}(t,t') & a,a' \in C \\ 0 & \text{otherwise} \end{cases}, \tag{76}$$

and analogous for Π_{corr}, where here we define the local propagators in the correlated subspace $a, a' \in C$ as

$$(G_{\text{loc,cor}})_{a,a'}(t,t') = G_{j,a;ja'}(t,t'), \quad (W_{\text{loc,cor}})_{a,a'}(t,t') = W_{j,a;ja'}(t,t'). \tag{77}$$

Like in conventional DMFT, we then introduce an electron-boson impurity model as an auxiliary device to evaluate these local contributions. The impurity action is

$$S_{\text{imp}} = \int_{\mathcal{C}} dtdt' \sum_{a,a'\in C} \bar{c}_a(t)\mathcal{G}^{-1}_{a,a'}(t,t')c_{a'}(t') - \frac{1}{2}\sum_{a,a'\in C}\int_{\mathcal{C}} dtdt'\, \varphi_a(t)\mathcal{W}^{-1}_{a,a'}(t,t')\varphi_{a'}(t') + i\sum_{a\in C}\int_{\mathcal{C}} dt\, \varphi_a(t)h_a(t)(t) + i\sum_{a\in C}\int_{\mathcal{C}} dt\, \varphi_a(t)n_a(t). \tag{78}$$

Here $\mathcal{G}$, $\mathcal{W}$ and h essentially define the noninteracting propagators of electrons and bosons in the impurity model; they are free parameters, which will be fixed by self-consistency conditions below. The last term is the electron-boson interaction, which is the same as in the lattice action (68). From the impurity model we measure the impurity correlation functions $\big\langle\varphi_a(t)\big\rangle_{\text{imp}}$, $(W_{\text{imp}})_{a,a'}(t,t') = i\big\langle\varphi_a(t)\varphi_{a'}(t')\big\rangle^{\text{con}}_{\text{imp}}$ and $(G_{\text{imp}})_{a,a'}(t,t') = -i\big\langle c_a(t)\bar{c}_{a'}(t')\big\rangle_{\text{imp}}$, and use the Dyson equation (understood as matrix equation in time and in the space C)

$$W^{-1}_{\text{imp}} = \mathcal{W}^{-1} - \Pi_{\text{imp}}, \tag{79}$$

$$G^{-1}_{\text{imp}} = \mathcal{G}^{-1} - \Big(\Sigma_{\text{imp}}(t,t') - i\delta(1,1')\langle\varphi(1)\rangle_{\text{imp}}\Big). \tag{80}$$

Here, we have treated the Hartree self-energy separately. If then we request a self-consistency between impurity quantities and local lattice quantities on the correlated subspace,

$$G_{\text{imp}} \stackrel{!}{=} G_{\text{loc,cor}}, \quad W_{\text{imp}} \stackrel{!}{=} W_{\text{loc,cor}}, \quad \big\langle\varphi_a(t)\big\rangle_{\text{imp}} = \big\langle\varphi_{j,a}(t)\big\rangle_{\text{imp}} \text{ for } a \in C, \tag{81}$$

it is guarantied that Σ_{imp} and Π_{imp} provide the sum of all local diagrams. Finally adding the correlated and GW self-energies gives the full approximation to the lattice self-energy,

$$\Sigma(1,1') = \Big[iG(1,1')W(1,1') - iG_{\text{loc,cor}}(1,1')W_{\text{loc,cor}}(1,1')\Big] + \Sigma_{\text{imp}}(1,1') - i\delta(1,1')\langle\varphi(1)\rangle, \tag{82}$$

$$\Pi(1,1') = \Big[-iG(1,1')G(1,1') + iG_{\text{loc,cor}}(1,1')G_{\text{loc,cor}}(1,1')\Big] + \Pi_{\text{imp}}. \tag{83}$$

Here in the GW self-energy and polarization we have subtracted the local contribution, which is already contained in Σ_{imp} and Π_{imp} respectively. Moreover, from the impurity model we take only the contribution beyond the Hartree mean-field term, because $\langle\varphi(1)\rangle$ is the same in the impurity and lattice due to the self-consistency.

This completes the description of the theory: One can start with a guess for the free parameters $\mathcal{W}$, $\mathcal{G}$ [or Δ], and h, solve the impurity model to extract Σ_{imp} and Π_{imp}, calculate the lattice self energies and polarization from Eqs. (82) and (83), from that calculate the lattice G and W, extract their local contributions, use the self-consistency condition to obtain a new guess for $\mathcal{W}$, $\mathcal{G}$, and h. In the actual implementation [47], there are some differences: First, the impurity model is transformed to a purely electronic model by integrating out the phonons,

$$S_{\text{imp}} = \int_{\mathcal{C}} dtdt' \sum_{a,a'\in C} \bar{c}_a(t)\tilde{\mathcal{G}}^{-1}_{a,a'}(t,t')c_{a'}(t') - \frac{1}{2}\sum_{a,a'\in C}\int_{\mathcal{C}} dtdt'\, n_a(t)\mathcal{W}_{a,a'}(t,t')n_{a'}(t'),$$

with the exact relations (cf. Eqs. (71) and (72))

$$W_{\text{imp}}(t,t') = \mathcal{W} + \mathcal{W}\chi_{\text{imp}}\mathcal{W}, \quad \langle\varphi\rangle_{\text{imp}} = i\int d1'\,\mathcal{W}(1,1')\langle n(1')\rangle. \tag{84}$$

Hence $\langle\varphi\rangle_{\text{imp}}$ and W_{imp} can be obtained by measuring χ_{imp} and $\langle n\rangle_{\text{imp}}$. This can be done, e.g., with the strong coupling equation as described around Eq. (64). Moreover, in the real-time Keldysh formalism, we again avoid directly solving for the inverse operators in discrete time (as in Eq. (79)), but transform all equations to well-behaved integral equations (see also the discussion around Eq. (61)). Finally, the bosonic propagators have time-local contributions, such as an instantaneous interaction $V\delta_C(t,t')$, which must be kept separately in the real time formalism. For a detailed discussion of these technical points, the reader is referred to Ref. [47].

4 Photodoping in Mott and charge-transfer insulators

4.1 Overview

In a Mott or charge-transfer insulator, electrons in a partially filled band get localized due to the Coulomb interaction. They still keep active spin and orbital degrees of freedom, leading to a large variety of magnetically and orbitally ordered low temperature phases, which can turn into unconventional metallic states or superconductors upon doping. DMFT and its extensions have been instrumental in the understanding of this physics, and non-equilibrium DMFT is therefore a natural starting point to investigate the non-equilibrium phenomena induced in Mott insulators driven by strong laser fields. The most straightforward way to excite the Mott insulator is to use a short laser pulse that is resonant to the charge gap. This will impulsively create mobile charge carriers, such as doubly occupied sites ("doublons") and holes in a single band Mott insulator, and will be followed by a sequence of dynamical processes:

Immediate response of the electronic structure: In a correlated electron system, the redistribution of charges between different orbitals leads to an almost immediate response of the electronic spectrum. Since the kinetic energy of photo-excited charges after an impulsive excitation is often high, the electrons will not form coherent quasiparticles on the shortest times, but the metallic character of the photo-excited state will become manifest in the formation of incoherent spectral weight within the Mott or charge-transfer gap. In a multi-band system, the inter-band Coulomb interaction can give rise to band shifts, and moreover the mobile charges will change the dynamic screening environment and therefore also interactions like the Hubbard U in the valence band. Below, we will discuss the change of the Hubbard U in a photo-excited charge-transfer insulator, which has been predicted theoretically [49,50] and recently measured using time-resolved Xray absorption [51].

Thermalization: Thermalization of a system implies that the properties of the system eventually approach the properties of a system in equilibrium, at a temperature T_f such that the total energy equals the thermal energy expectation value $E_{\text{th}}(T_f)$ at temperature T_f, $\langle H(t)\rangle \equiv E_{\text{tot}} \stackrel{!}{=} E_{\text{th}}(T_f)$. In a correlated electron system, one can expect that the electronic system can thermalize before passing on a substantial fraction of its energy to other degrees of freedom (phonons),

leading to the formation of a correlated electron liquid at high temperature, which subsequently cools down by coupling to the lattice. While such a "hot electron picture" is quite obvious and has been employed ever since in the investigation of photo-induced solids, the correlated nature of the state brings in few nontrivial aspects: The high-temperature state, with temperature of the order of the electronic band width, can have peculiar spectral and transport properties, such as bad metallic behavior [52, 28]. In equilibrium, the same state would not be accessible because also the lattice would have to be heated, and such high temperature correlated fermion liquids are therefore rather accessible in cold atom quantum simulators [53]. The understanding of their dynamics at short times and high energies offers the opportunity for a detailed and systematic comparison of theory and experiment.

Prethermal photo-doped states: In the presence of the Mott or charge-transfer gap, full thermalization can be inhibited for relatively long times. The thermalization of a single-band photo-doped Mott insulator has been analyzed within DMFT in Ref. [54], by calculating the double occupancy and the spectral functions after the pulse. One finds that the double occupancy increases during the pulse, and subsequently shows an exponential relaxation to a new final value, from which the thermalization time can be extracted. This timescale strongly depends on U, and ranges from few hopping times (few femtoseconds for a typical eV bandwidth) in the correlated metal, to thousands of hopping times in the Mott phase. The fast thermalization in a small gap Mott insulator has been experimentally investigated in 1T-TaS_2 [55]. At large U, instead, the double occupancy D can be viewed as an almost conserved quantity, so that one can expect the electronic state to be described as a quasi-thermal state with a thermodynamic variable D in addition to the total particle number N and the total energy E. In fact, simulations for the one-band Hubbard model show that the system quickly establishes a distribution function with a universal form, given by a Fermi function with separate chemical potentials in the upper and lower Hubbard band [28]. This universal form hints at a description in terms of few additional slow variables. Upon energy transfer to the lattice (or to spins [44] and other degrees of freedom), the state may acquire a low temperature but still have a substantial fraction of additional doubly occupied sites and holes, i.e, it is a cold correlated liquid of spins (singly occupied sites), holes and doublons. The quasi-steady properties of such photo-doped states may support phases different from those in the equilibrium phase diagram. They can be explored by taking the equilibrium states of a suitable model in which D is turned into an exactly conserved quantity (for the Hubbard model, this is a generalized the t-J model, in which charge recombination processes are projected out [57, 16]). Alternatively, one can try to work within the Hubbard model and establish the quasi-steady state as a true steady state under the application of suitable reservoirs [56]. In both cases, for the Hubbard model, η-pairing superconductivity is found for strong photo-excitation [57, 16].

4.2 Electronic structure in a photo-excited charge-transfer insulator

Finally, we briefly review the first application of the non-equilibrium GW+DMFT to a realistic material simulation [49]. We focus on a three-band model for a charge-transfer insulator. It

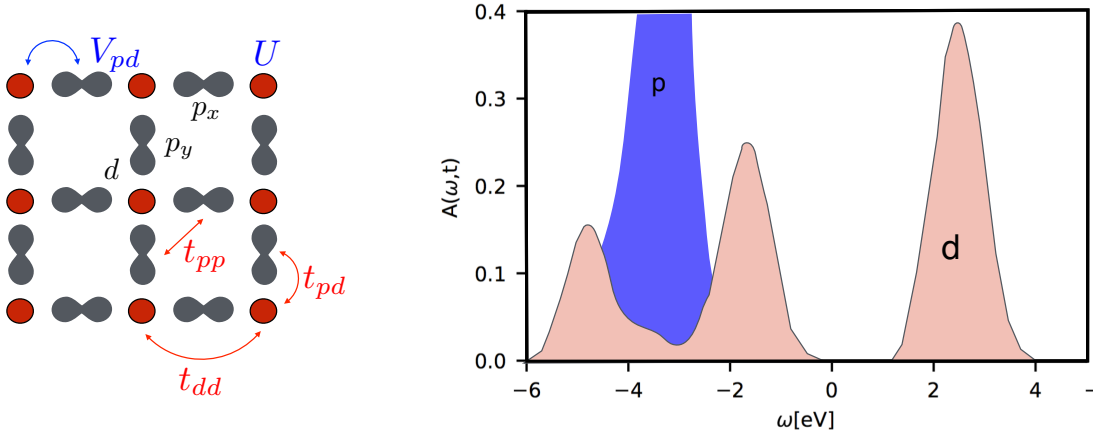

Fig. 3: *Left: 3-band Emery model for a charge-transfer insulator. Right: p and d spectral functions in equilibrium, as obtained with GW+DMFT. Adapted from Ref. [49]*

.

describes a two-dimensional cubic lattice with two ligand orbitals p_x and p_y and one d orbital per unit cell (see Fig. 3, left). We take into account a nearest neighbor p-d hopping $t_{pd} = 0.4\,\text{eV}$, a direct d-d hopping $t_{dd} = -0.1\,\text{eV}$, a charge-transfer energy (energy difference $\epsilon_p - \epsilon_d = -2\,\text{eV}$), a inter-site p-d density-density interaction $V_{pd} = 2\,\text{eV}$, and a local Hubbard interaction on the d orbitals, $U_{dd} = 8\,\text{eV}$. The parameters are determined to best match the spectrum for the cuprate LSCO. With 5 electrons per unit cell, the system has a nominally half-filled d band, which is split into upper and lower Hubbard band due to the large U_{dd}. The model is solved in and out of equilibrium with the GW+DMFT formalism (see Sec. 3.2), using the non-crossing approximation as an impurity solver (Sec. 3.3). The local spectral function in equilibrium ($\beta = 5$) is shown in Fig. 3, right panel; one can clearly distinguish the upper and lower Hubbard band in the d-related spectrum, where the lower Hubbard band hybridizes with the p bands.

We now simulate the time-dependent spectral and occupation functions during and after the excitation of the system with a short electric field pulse. The pulse couples to the model via both a Peierls phase and dipolar matrix elements (for details see [47]). The electric field has the form

$$E(t) = E_0 e^{-4.6(t-t_0)^2/t_0^2} \sin(\Omega(t-t_0)), \tag{85}$$

with a frequency Ω that is varied below mostly resonant to the charge-transfer gap, and a duration of roughly two cycles ($t_0 = 4\pi/\Omega$). It is polarized along the (11) direction, and the amplitude is adapted to achieve a certain excitation density.

Figure 4a) shows the spectrum shortly after an excitation with about 5% photo-doping (measured by the change of the double occupancy after the pulse). Time-resolved spectra are obtained from the Wigner transform $A_\alpha(\omega, t) = -\frac{1}{\pi} \operatorname{Im} G^R_\alpha(t, \omega + i0)$ for $\alpha = p, d$. One can clearly see a shift and broadening of all bands. To further elucidate the origin of these band structure changes, one can switch off the nonlocal GW self-energies and polarizations, and keep only the Hartree and Fock self-energies (HF+DMFT) in the simulation. In this case, the band shifts on the d band can mainly be understood as a consequence of the mean-field p-d interaction, which

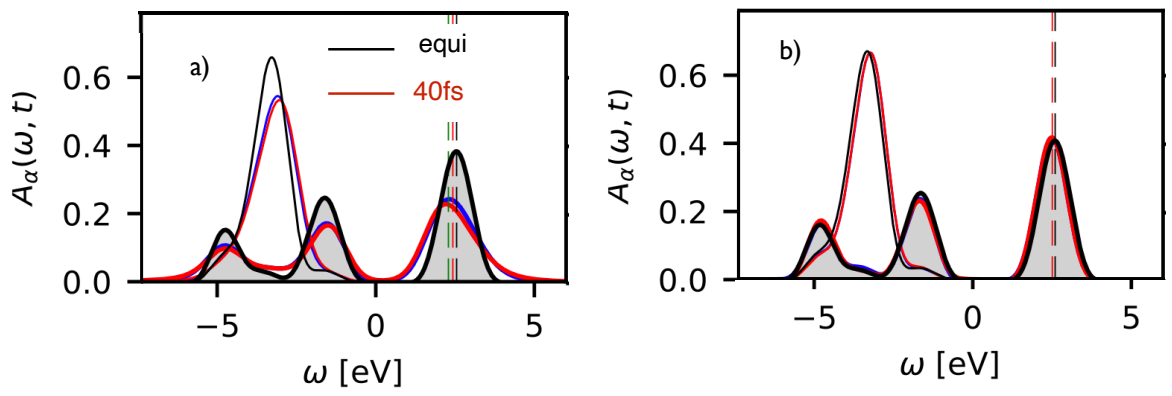

Fig. 4: *a) Spectra after photo-excitation of the Emery model in equilibrium (black lines) and shortly after the excitation ($40\,fs$, red). The pulse frequency $\Omega = 6\,eV$ is resonant to an excitation across the gap, and the excitation density (change in the doubly occupancy on the d-sites) is about 5%. One finds a significant broadening and shift of the bands. b) Same parameters, but taking only the static Hartree and Fock diagrams beyond DMFT into account. Adapted from Ref. [49]*

.

implies a shift of the d level given by $\delta\epsilon_d = V_{pd}\,\delta\langle n_d\rangle$ depending on the change $\delta\langle n_d\rangle$ of the p occupation. The result is shown in Fig. 4b). The center of mass shift of the upper Hubbard band turns out to be about a factor two larger in the GW+DMFT simulation as compared to the HF+DMFT simulation. This shows a significant quantitative role of the dynamic screening processes due to the long-range interaction, which are captured by the GW formalism. In the language of GW+DMFT, one can understand these screening processes in turns of a reduction of the onsite interaction U in the photo-excited state. Similar band shifts after photo-excitation have been reported for LSCO using XAS from a core level [51], which have also been interpreted as a dynamic screening of the Hubbard U. Because of the strong core-valence excitonic character of the final state in XAS, XAS cannot directly be linked to the single-particle spectral function presented in the present study. To get a quantitative interpretation of the experiment it would be interesting to compute the XAS within GW+DMFT, along the lines presented in Ref. [58].

In addition to the quantitative relevance of the dynamic screening processes, we observe that the spectrum is strongly broadened in the GW+DMFT simulation, while band shifts are more or less rigid within HF+DMFT. The reason is that the interaction of electrons with the nonlocal dynamic charge fluctuations, which is captured by the GW diagrams, opens a new scattering channel in the photo-doped state. For the same reason, also the dynamics of the occupation functions is very different in the two cases (not shown here, see Ref. [49]): The interaction of electrons with charge fluctuations leads to a rapid relaxation of the photo-doped electron and hole distributions to the bottom of the upper Hubbard band and the top of the hybrid p/d bands, respectively, whereas this relaxation would require the coupling to an additional bath of phonons in the HF+DMFT simulation. Hence, we see that keeping the dynamical nonlocal fluctuations is essential for an accurate description of photo-doped states.

5 Outlook

In these notes we have reviewed the theoretical basis for a description of correlated electron systems out of equilibrium using the non-equilibrium extension of DMFT and GW+DMFT. While such simulations have been used to understand many aspects of photo-exited states in solids, a desirable future development will be to bring the non-equilibrium formalism to a similar level of quantitative predictive power as the equilibrium DMFT formalism. The main challenge in this direction is the solution of the impurity problem. There are currently no non-perturbative impurity solvers which work at long times. While low-order variants of the strong-coupling expansion, such as NCA, can be applied very flexibly within the Mott phase, they become increasingly inaccurate for correlated metallic phases. An interesting perspective are given by the application of the non-perturbative methods (QMC [41] and Hamiltonian-based solvers [35]). In the near future, it might in particular become feasible to use these non-perturbative techniques for a study of non-equilibrium steady states, which then can provide an effective description of long-lived photo-excited phases [16, 56], or be elevated to study slow time-evolution using quantum Boltzmann equations based on steady-state DMFT [32].

Acknowledgements

I acknowledge funding from the ERC via starting grant No. 716648.

References

[1] C. Giannetti, M. Capone, D. Fausti, M. Fabrizio, F. Parmigiani, and D. Mihailovic, Adv. in Phys. **65**, 58 (2016)

[2] D. Basov, R.D. Averitt, and D. Hsieh, Nat. Mater. **16**, 1077 (2017)

[3] A. de la Torre, D.M. Kennes, M. Claassen, S. Gerber, J.W. McIver, and M.A. Sentef, Rev. Mod. Phys. **93**, 041002 (2021)

[4] D. Wegkamp *et al.*, Phys. Rev. Lett. **113**, 216401 (2014)

[5] S. Mor *et al.*, Phys. Rev. Lett. **119**, 086401 (2017)

[6] A. de la Torre *et al.*, Comm. Phys. **5**, 35 (2022)

[7] M. Först, C. Manzoni, S. Kaiser, Y. Tomioka, Y. Tokura, R. Merlin, and A. Cavalleri, Nat. Phys. **7**, 854 (2011)

[8] T. Oka and H. Aoki, Phys. Rev. B **79**, 081406(R) (2009)

[9] J.W. McIver, B. Schulte, F.-U. Stein, T. Matsuyama, G. Jotzu, G. Meier, and A. Cavalleri, Nat. Phys. **16**, 38 (2020)

[10] T. Oka and S. Kitamura, Annu. Rev. Condens. Matter Phys. **10**, 387 (2019)

[11] A. Georges, G. Kotliar, W. Krauth, and M.J. Rozenberg, Rev. Mod. Phys. **68**, 13 (1996)

[12] P. Schmidt, and H. Monien, arXiv:cond-mat/0202046

[13] J.K. Freericks, V.M. Turkowski, and V. Zlatić, Phys. Rev. Lett. **97**, 266408 (2006)

[14] H. Aoki, N. Tsuji, M. Eckstein, M. Kollar, T. Oka, and Ph. Werner, Rev. Mod. Phys. **86**, 779 (2014)

[15] J. Li, H.U.R. Strand, P. Werner, and M. Eckstein, Nat. Comm. **9**, 4581 (2018)

[16] J. Li, D. Golez, Ph. Werner, and M. Eckstein, Phys. Rev. B **102**, 165136 (2020)

[17] Y. Murakami, M. Eckstein, and Ph. Werner, Phys. Rev. Lett. **121**, 057405 (2018)

[18] N. Dasari, J. Li, Ph. Werner and M. Eckstein, Phys. Rev. B **101**, 161107 (2020)

[19] M. Eckstein: Ch. 15 in E. Pavarini, E. Koch, D. Vollhardt, and A. Lichtenstein (eds.): *DMFT: From Infinite Dimensions to Real Materials*
Modeling and Simulation vol. 8 (Forschungszentrum Jülich, 2018)
`http://www.cond-mat.de/events/correl18`

[20] M. Schüler, D. Golez, Y. Murakami, N. Bittner, A. Hermann, H.U.R. Strand, Ph. Werner and M. Eckstein, Comp. Phys. Commun. **257**, 107484 (2020)

[21] A. Kamenev: *Field Theory of Non-Equilibrium Systems* (Cambridge University Press, 2011)

[22] G. Stefaniccu and R. v. Leeuwen: *Nonequilibrium Many-Body Theory of Quantum Systems* (Cambridge University Press, 2013)

[23] J.K. Freericks, H.R. Krishnamurthy, and Th. Pruschke, Phys. Rev. Lett. **102**, 136401 (2009)

[24] H. Haug, and A. Jauho: *Quantum Kinetics in Transport and Optics of Semiconductors* (Springer, 2008)

[25] F. Randi, D. Fausti, and M. Eckstein, Phys. Rev. B **95**, 115132 (2017)

[26] K. Balzer and M. Bonitz: *Nonequilibrium Green's Functions Approach to Inhomogeneous Systems* (Springer, 2008)

[27] Ch. Stahl, N. Dasari, J. Li, A. Picano, Ph. Werner, M. Eckstein, Phys. Rev. B **105**, 115146 (2022)

[28] N. Dasari, J. Li, Ph. Werner, and M. Eckstein, Phys. Rev. B **103**, 201116 (2021)

[29] A. Picano and M. Eckstein, Phys. Rev. B **103**, 165118 (2021)

[30] J. Kaye and D. Golež, SciPost Phys. **10**, 91 (2021)

[31] N. Schlünzen, J.-P. Joost, and M. Bonitz, Phys. Rev. Lett. **124**, 076601 (2020)

[32] A. Picano, J. Li, and M. Eckstein, Phys. Rev. B **104**, 085108 (2021)

[33] M. Wais, M. Eckstein, R. Fischer, P. Werner, M. Battiato, and K. Held, arXiv:1806.02570

[34] W. Metzner and D. Vollhardt, Phys. Rev. Lett. **62**, 324 (1989)

[35] Ch. Gramsch, K. Balzer, M. Eckstein, and M. Kollar, Phys. Rev. B **88**, 235106 (2013)

[36] F.A. Wolf, I.P. McCulloch, and U. Schollwöck, Phys. Rev. B **90**, 235131 (2014)

[37] K. Balzer, F.A. Wolf, I.P. McCulloch, Ph. Werner, and M. Eckstein, Phys. Rev. X **5**, 031039 (2015)

[38] E. Arrigoni, M. Knap, and W. von der Linden, Phys. Rev. Lett. **110**, 086403 (2013)

[39] E. Gull, A.J. Millis, A. Lichtenstein, A.N. Rubtsov, M. Troyer, and Ph. Werner, Rev. Mod. Phys. **83**, 349 (2011)

[40] M. Eckstein, M. Kollar, and Ph. Werner, Phys. Rev. Lett. **103**, 056403 (2009)

[41] G. Cohen, E. Gull, D.R. Reichman, and A.J. Millis, Phys. Rev. Lett. **115**, 266802 (2015)

[42] A.J. Kim, J. Li, M. Eckstein, and Ph. Werner, arXiv:2204.13562

[43] M. Eckstein and Ph. Werner, Phys. Rev. B **82**, 115115 (2010)

[44] M. Eckstein and Ph. Werner, Sci. Rep. **6**, 21235 (2016)

[45] S. Biermann, F. Aryasetiawan, and A. Georges, Phys. Rev. Lett. **90**, 086402 (2003)

[46] K. Held, Ch. 13 in E. Pavarini, E. Koch, D. Vollhardt, and A. Lichtenstein (eds.):
The LDA+DMFT Approach to Strongly Correlated Materials
Modeling and Simulation vol. 1, (Forschungszentrum Jülich, 2011)
`http://www.cond-mat.de/events/correl11`

[47] D. Golez, M. Ecksteoin, Ph. Werner, Phys. Rev. B **100**, 235117 (2019)

[48] L. Hedin, Phys. Rev. **139**, A796 (1965)

[49] D. Golež, L. Boehnke, M. Eckstein, and P. Werner, Phys. Rev. B **100**, 041111 (2019)

[50] N. Tancogne-Dejean, M.A. Sentef, and A. Rubio, Phys. Rev. Lett. **121**, 097402 (2018)

[51] D.R. Baykusheva *et al.*, Phys. Rev. X **12**, 011013 (2022)

[52] X. Deng, J. Mravlje, R. Zitko, M. Ferrero, G. Kotliar, and A. Georges,
Phys. Rev. Lett. **110**, 086401 (2013)

[53] P.T. Brown *et al.*, Science **363**, 379 (2018)

[54] M. Eckstein and Ph. Werner, Phys. Rev. B **84**, 035122 (2011)

[55] M. Ligges *et al.*, Phys. Rev. Lett. **120**, 166401 (2018)

[56] J. Li and M. Eckstein, Phys. Rev. B **103**, 045133 (2021)

[57] Y. Murakami, Sh. Takayoshi, T. Kaneko, Zh. Sun, D. Golež, A.J. Millis, and Ph. Werner,
Comm. Phys. **5**, 23 (2022)

[58] Ph. Werner, D. Golež and M. Eckstein, arXiv:2204.06762